



Cholesterol Solubility Limit in Lipid Membranes probed by Small Angle Neutron Scattering and MD simulations

Journal:	<i>Soft Matter</i>
Manuscript ID:	SM-ART-06-2014-001219.R2
Article Type:	Paper
Date Submitted by the Author:	30-Sep-2014
Complete List of Authors:	Perez-Salas, Ursula; University of Illinois - Chicago, Physics Garg, Sumit; Berg LLC, Biophysics Castro-Roman, Francisco; Centro de Investigación y de Estudios Avanzados del IPN, Porcar, Lionel; Institut Laue-Langevin, Large Scale Structure Group Butler, Paul; NIST, Ceneter for Neutron Research Bautista, Pedro; Centro de Investigación y de Estudios Avanzados del IPN, Krzyzanowski, Natalie; University of Illinois Chicago, Physics

Cite this: DOI: 10.1039/c0xx00000x

www.rsc.org/xxxxxx

ARTICLE TYPE

Cholesterol Solubility Limit in Lipid Membranes probed by Small Angle Neutron Scattering and MD simulations

Sumit Garg,^{‡a,b} Francisco Castro-Roman,^c Lionel Porcar,^{d,f} Paul Butler,^{e,f} Pedro Jesus Bautista,^c Natalie Krzyzanowski,^b and Ursula Perez-Salas^{*b,a}

⁵ Received (in XXX, XXX) Xth XXXXXXXXX 20XX, Accepted Xth XXXXXXXXX 20XX

DOI: 10.1039/ The solubility limits of cholesterol in small unilamellar vesicles made of POPS and POPC were probed using Small Angle Neutron Scattering (SANS) and coarse grained (CG) molecular dynamics (MD) simulations. SANS, being non-invasive, allowed the direct and quantitative measurement of cholesterol in intact vesicles. Our experimental measurements reveal a 61% mole fraction solubility limit of cholesterol in POPC, consistent with previous studies. However, in POPS the solubility limit of cholesterol is found to be 73% mole fraction. Previous work reports solubility limits of cholesterol in POPS varying significantly, ranging from 36% up to 66%. The CG MD simulations are in remarkable quantitative agreement with our experimental results showing similar solubility limits. Further, neither experiments or simulations show evidence of stable nanodomains of cholesterol in POPS membranes as suggested in some previous reports.

Cholesterol is a major component of mammalian cells and plays a critical role in permeability, rigidity, dynamics and interaction with the cytoskeleton.¹ However, excess cholesterol, specifically in the crystalline phase, can be toxic.^{2, 3} Cholesterol crystals are directly implicated in several pathological conditions, including coronary artery disease, which is characterized by the narrowing of the inner blood vessel walls by the deposition of plaques containing cholesterol crystals.⁴

For the past few decades the appearance of cholesterol crystals, as measured by x-ray diffraction, NMR and calorimetry, has been linked to cholesterol's solubility limit in lipid membranes.⁵⁻⁸ Here, the solubility limit is defined as the concentration beyond which the membrane is no longer able to hold further cholesterol and is therefore expelled from the membrane forming crystalline aggregates. Reported solubility limits of cholesterol in lipid membranes depend on the nature of the lipids, and vary from a few mole percent to up to ~70% mole fraction.^{5-7, 9-11} In particular POPS, which is highly enriched in the inner leaflet of the outer membrane of eukaryotic cells¹³, has reported cholesterol solubilities that vary from 36% mole fraction to 66% mole fraction. Moreover the more accepted lower end of the range of 36% mole fraction cholesterol¹² is very similar to the typical cholesterol concentration in the cellular membrane. Most other relevant lipids have significantly higher solubility limits suggesting a possible role for POPS in pathological crystal formation. To better understand any such potential role, however, requires an accurate measure of cholesterol's solubility limits.

Here we present a combined study using small angle neutron scattering (SANS) and coarse-grained (CG) molecular dynamics (MD) simulations to accurately correlate the molecular description of cholesterol's solubility in lipid membranes with those measured experimentally. Besides POPS, we also studied

cholesterol's solubility in POPC lipid membranes, another important lipid in the outer cellular membrane.¹³ The reported cholesterol solubilities in POPC membranes are much more consistent at 55 to ~63% mole fraction.⁵

SANS, being a non-invasive probe, can directly detect the extent to which a single membrane can incorporate cholesterol into its bilayer by taking advantage of the vastly different neutron contrast between hydrogenated and deuterated materials. Using deuterated lipids and appropriate mixtures of water and heavy water it was possible to contrast match the lipids to the solvent thus highlighting only cholesterol. We found that the maximum solubility of cholesterol in POPC is 61% mole fraction, as previously shown, while in POPS it is 73% mole fraction, which is a significantly higher value than previously reported.

CG MD simulations were carried out using the MARTINI force field implemented within the Gromacs 4.0.5 package for ensembles of varying box sizes, ranging from 12 nm to 20 nm per side. The simulations explored the behavior of POPC and POPS bilayers with varying amounts of cholesterol, from 0 to 90% mole fraction. Coarse-grained lipid and cholesterol molecules spontaneously self-assembled, and equilibrated into typical fluid planar bilayers. Cholesterol preferentially sits at its usual position where the hydroxyl group locates near the aqueous interface and the sterol parallel to the bilayer normal. No evidence of lateral cholesterol-rich domains was found in the simulations, even at the highest cholesterol content. The saturation limit for cholesterol in the leaflets of both POPC and POPS bilayers agrees well with our SANS experimental results.

Results

Small Angle Scattering

In SANS, the scattered intensity, $I(Q)$, for a solution of lipid

vesicles depends on the vesicle's form factor $P(Q)$, the vesicle's volume $V_{vesicle}$, the vesicle's number density, n , and the difference, or contrast, between the scattering length density of the vesicle's membrane ($\rho_{vesicle}$) and the solvent ($\rho_{solvent}$):

$$I(Q) = nV_{vesicle}^2(\rho_{vesicle} - \rho_{solvent})^2P(Q)_{vesicle} + I_{incoherent} \quad (1)$$

Because $\rho_{vesicle}$ is the volume fraction weighted contributions of its components, ρ_{lipid} and $\rho_{cholesterol}$, it is possible to choose ρ_{lipid} = $\rho_{solvent}$, such that equation 1 can be rewritten as:

$$I(Q) = nV_{vesicle}^2x^2(\rho_{cholesterol} - \rho_{solvent})^2P(Q)_{vesicle} + I_{incoherent} \quad (2)$$

where x corresponds to the volume fraction of cholesterol in the vesicle. Therefore, when the lipids are contrast matched to the solvent the measured scattered intensity increases quadratically with cholesterol content in the vesicles.

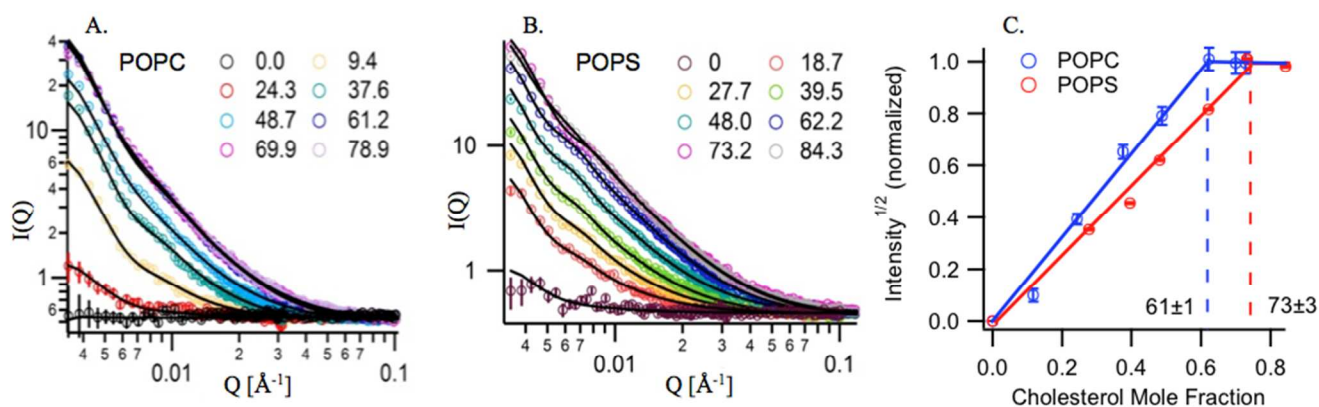


Figure 1. A. and B. I vs. Q curves for 100nm extruded vesicles made of cholesterol/POPC (A) and cholesterol/POPS (B) membranes for increasing cholesterol mole fraction. Fits of the data were done using a vesicle form factor. C. $Intensity^{1/2} = [(I_{lowQ} - I_{incoherent}) / I_{max}]^{1/2}$ as a function of the nominal mole fraction of cholesterol present in the vesicles. Unless otherwise stated, error bars represent one sigma.

Figures 1A and 1B show the absolute scattered intensity I vs Q curves for POPC and POPS membranes with varying cholesterol concentrations in lipid contrast-matched conditions. As expected, the intensity increases as cholesterol concentration increases up to a threshold cholesterol concentration, above which no further change in the scattering curve is observed. Using the vesicle form factor to fit the data (as shown in Figures 1A and 1B) we determined that indeed the variation in intensity is due solely to the corresponding fractions of cholesterol in the membranes. Taking the square root of the integrated, coherent intensity (proportional to the fraction of cholesterol in the vesicle as per equation 2) between 0.004\AA^{-1} to 0.005\AA^{-1} , and plotting it as a function of fraction of cholesterol (Figure-1C) dramatically illustrates a sharp solubility limit occurring at 61 ± 1 mole % cholesterol in POPC and 73 ± 3 mole % cholesterol in POPS.

Our results in POPC are consistent with Huang *et al.* who find the cholesterol solubility limit to be between 55 to 63 mole % - reflecting differences obtained depending on the sample preparation method used.⁵ The 73% mole fraction solubility limit of cholesterol in POPS membranes on the other hand stands in stark contrast to the accepted solubility limit of 36% mole fraction.^{11, 12, 14} Even a variation of up to 8% in the solubility limit

of cholesterol in POPS due to the sample preparation cannot explain such discrepancy. While one study has suggested that the solubility limit of cholesterol in POPS must be higher than 50% mole fraction,⁹ only the work by Raguz *et al.* using electron paramagnetic resonance (EPR) suggests a saturation of cholesterol on the order of 66% mole fraction.¹⁵

Coarse-grained MD simulations

Our CG MD simulations are surprisingly in near quantitative agreement with the SANS work. Fully equilibrated simulation snapshots for increasing cholesterol concentration in POPS are shown in Figure 2A. From visual inspection it is seen that the concentration hydroxyl groups in the plane of the membrane stops increasing around 70% mole fraction of cholesterol, even while the concentration of cholesterol continues to increase. This plateau is suggestive of a saturation limit of cholesterol in the

bilayer leaflets.

Looking closely at snapshots/movies of the simulations one can always pick out a few cholesterol molecules in close proximity. This number increases from a couple to less than a dozen at very high cholesterol concentrations. Whether these represent true transient clusters, as some papers suggest exist, or are simply the natural consequence of thermal motion in a highly concentrated particle system, is a more complex question probably beyond the level the simulations presented here can unambiguously ascertain. More importantly however, the difference between the lipid head groups (PC and PS) does not seem to influence the interaction potentials enough to affect cholesterol's arrangement or saturation process. Work is in progress to investigate if the dynamic behaviour of these systems affects cholesterol transport.

Discussion

SANS measurements showing the increasing accumulation of cholesterol in the membrane (as shown in Figures 1A and 1B) are insensitive to the structural state of the cholesterol as long as it is inserted in the bilayer. These measurements thus give the total cholesterol content in the membrane, and consequently the

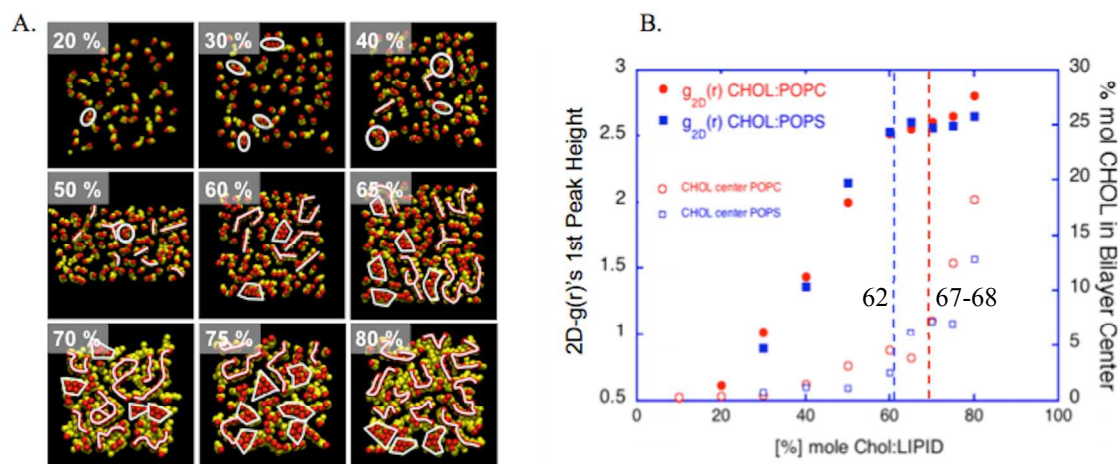


Figure 2. A. In-plane view of the cholesterol molecules for one leaflet of coarse grained simulated POPS bilayers with different cholesterol mole fractions. Lines connecting cholesterol hydroxyl groups (in red) highlight small dynamic “clusters” and thread-like groupings. B. Height of the first peak of the 2D radial distribution function, $g(r)$, as a function of cholesterol mole fraction; also plotted is the fraction of cholesterol found in between the lipid leaflets and in a horizontal orientation parallel to the bilayer plane (dash lines mark the saturation limits of the membranes’ leaflets).

membrane solubility limit, but say nothing about the lateral organization of that cholesterol in the lipid leaflet. On the other hand, under contrast matching conditions for the whole vesicle, SANS can be used to detect domains.¹⁶ In a separate test, however, we failed to detect any domains within our ~5nm resolution.

While our simulations show some evidence for possible dynamic inhomogeneities in the distribution of cholesterol within the bilayer, there is certainly no evidence for stable, “large” scale cholesterol domains or evidence of a seed for cholesterol crystals up to 90% mole fraction of cholesterol supporting our SANS results. Small dynamic “clusters” grouping a few cholesterol molecules start to appear as low as 20% mole fraction (Figure 2A). Above 60% thread-like microstructures become noticeable and at 70% mole fraction cholesterol clusters of up to 8 molecules and thread-like structures coexist and their relative fraction or ratio does not change when cholesterol concentration increases. Both kinds of structures have been observed by others: using all-atom MD simulations O’Connor *et al.* observed cholesterol-only nano domains in DMPC at 66% mole fraction while Miao *et al.* reported threadlike cholesterol structures in DPPC-like lipid membranes using Monte Carlo simulations.^{17, 18} Whether there is any significance to such “structures” beyond what would be expected for highly concentrated particles in 2D in constant thermal motion is beyond the scope of this paper. However it is clear that there are no long lived or even significantly sized domains forming that could be considered “effective crystals.”

Beyond the saturation limit, our SANS data, as in EPR studies,^{15, 19} show that additional cholesterol is not incorporated into the lipid leaflet. Further, the thickness of the bilayer with the addition of cholesterol as measured by SANS shows no indication that cholesterol is accumulating in the bilayer center prior to this saturation (supplemental information Figure S1).^{20, 21}

Thus it is clear that the excess cholesterol must be in the solution as microcrystals or precipitated out, since cholesterol’s solubility in water is too low to accommodate the excess cholesterol as dissolved cholesterol monomers.

It is well known that current MD simulation methods and the state of the art MARTINI force fields do not adequately describe cholesterol in an aqueous environment and cannot, for example, organize cholesterol into cholesterol crystals. Indeed, recent all atom simulations by Plesnar *et al.*, studying pre-assembled 100% cholesterol bilayers failed to obtain cholesterol crystals under hydrated conditions; they produced a rather loose fluid-like cholesterol bilayer.²² We have also investigated the formation of cholesterol aggregates under hydrated conditions and failed to obtain any – either bilayered or 3D – crystalline structures using the MARTINI forces field. There is furthermore an often expressed concern with the MARTINI force fields that they tend to place cholesterol into the bilayer interior. Thus the simulation results, above the solubility limit, are somewhat beyond the validity of currently available simulations to address. However, it is interesting to note that in our simulations only relatively small amounts of cholesterol were relegated to the centre of the bilayer interior until the solubility limit. Once the leaflets become saturated in cholesterol, the simulation has to eject excess cholesterol and it does so by accumulating this excess into the inter-leaflet space rather than ejecting it to the aqueous environment. Given the simulation’s inability to create tight aggregates of cholesterol in water along with the low aqueous solubility of cholesterol, it is clear that the simulations are simply moving excess cholesterol to the lowest energy region it is able to find. Thus the “kink” in the number of cholesterol molecules located in the center of the bilayer (Figure 2B) combined with the variation of the height of the first order peak of the 2D pair correlation function provides a means to obtain quantitatively a solubility limit of 62% mole fraction of cholesterol in POPC (compared to 61±1 from SANS) and a somewhat higher limit of

67-68% mole fraction of cholesterol (compared to 73 ± 3 from SANS) in POPS membranes. Even this slightly larger difference for POPS is within the expected variations based on sample prep and provides a remarkable agreement between our experiments and the simulations.

Conclusions

This study provides some significant new insights into cholesterol solubility, which was found to be high with no evidence of large in-membrane domains. This is particularly striking in the case of POPS membranes, since POPS is found enriching the cytoplasmic leaflet of cells in the human nervous system. Much work remains to understand the delicate balance that leads to the pathological 3D cholesterol crystals found in atherosclerotic plaques where membrane conformation, like multilamellar stacks, may play an important role. Indeed, small differences in the host lipid itself will clearly be a factor as suggested by Ziblat *et al.*, who found that ceramide promptly formed these 3D cholesterol crystals while DPPC and sphingomyelin did not.²³

Current work is ongoing to improve the force fields used in both all atoms and coarse grained simulations. For example, Lim *et al.* recently proposed a new cholesterol force field for all atom simulations and they state that it should remove cholesterol's preference for the centre of the bilayer, though it has not been shown to be the case yet.²⁴ For CG simulations Daily *et al.* have made changes to the MARTINI force field which has slightly improved the agreement of the simulations with experimentally measured properties of POPC membranes such as the bilayer's thickness variation with added cholesterol.²⁵ Other issues seem to have appeared though, like an excessive associativity between cholesterol molecules. Thus a detailed understanding above the solubility limit remains inaccessible to simulations and thus cannot yet yield molecular level details of the onset of cholesterol crystal formation upon reaching and crossing the solubility limit. However, the solubility limit of cholesterol at normal physiologically relevant concentrations in POPS enriched leaflets should not be a predominant driving force for clinically relevant crystal formation.

Materials and methods

Preparation of unilamellar lipid vesicles.

1-Palmitoyl(d31)-2-oleoyl-sn-glycero-3-phosphocholine (dPOPC) and 1-Palmitoyl(d31)-2-oleoyl-sn-glycero-3-phospho-L-serine (dPOPS) (both with only the Palmitoyl chain deuterated), cholesterol and the extruder setup were purchased from AVANTI POLAR LIPIDS (Alabaster, AL). We prepared 100nm (10mg/ml) diameter vesicles using single deuterated tail POPC and POPS lipids with increasing amounts of cholesterol, prepared via extrusion. ‡

The lipids, in powder form, were used as received. The desired lipid and cholesterol ratios were mixed as dry powders and then dissolved in chloroform to ensure the proper mixing of cholesterol and lipids. The chloroform was removed by a flow of nitrogen followed by vacuum overnight at 50°C. These mixtures were hydrated with solvents made of appropriate ratios of D2O and H2O to achieve the correct neutron contrast match point for

the lipids (see SANS Contrast Matching section below). Finally, these aqueous solutions were extruded through 100 nm polycarbonate filters to produce small unilamellar vesicles. The stability of the vesicles was verified from the stability of the small angle neutron scattering (SANS) patterns at 20°C and 60°C as well as through the course of a few days.

Small Angle Scattering (SANS) experiment

Small Angle Scattering (SANS) measurements were performed on the NG3 30 m SANS instruments at the National Institute of Standard and Technology Center for Neutron Research (NIST-CNR), Gaithersburg, MD and on D22 at the Institut Laue Langevin Grenoble. Measurements covered a Q-range of $0.003 < Q < 0.583 \text{ \AA}^{-1}$. Here Q is the magnitude of the scattering vector given by $Q = 4\pi \sin(\theta/2)/\lambda$, where θ is the scattering angle and λ is the neutron wavelength. The wavelength used was 6 Å. Data was collected using a 2-D detector and reduced using the reduction packages provided by NIST-CNR. ‡‡

SANS Contrast Matching

In this study, we measured the solubility of cholesterol in lipid membranes made of deuterated POPC (dPOPC) and deuterated POPS (dPOPS) because the scattering length density (SLD) of hydrogenated lipids is nearly the same to that of cholesterol and would thus render the measurement of the solubility of cholesterol impossible. The aqueous medium was adjusted to a D₂O/H₂O ratio with the same SLD as that of the lipid (dPOPC or dPOPS respectively). This ratio is obtained by measuring the scattering intensity of lipid vesicles (devoid of cholesterol) with varying ratios of D₂O/H₂O ratios. The resulting intensities are plotted as a function of D₂O (or H₂O) content and extrapolated to the percent at which the intensity becomes zero. This percent is rechecked to confirm that the scattering yields a completely flat SANS pattern, and it is shown in Figure 1. The contrast match points were found to be 48.6% D₂O for dPOPC and 55.8% D₂O for dPOPS.

MD simulations

Standard simulation parameters associated with the MARTINI force field and polarizable water model were used. The Lennard-Jones potential was shifted from 0.9 to 1.2 nm and cut off after 1.2 nm. The Coulomb potential was shifted from 0 to 1.2 nm with a relative dielectric constant of 2.5. A 20 fs integration time step was used in all simulations with neighbour list updates every 10 steps. Atom overlaps were removed using the steepest descent algorithm. The system was coupled to a pressure bath (1 atm, $\tau_p = 3$ ps) using the semi-isotropic coupling scheme. Different molecule types were coupled separately to a heat bath at 303 K using the Berendsen temperature coupling ($\tau_T = 1$ ps). The simulated boxes ranged in sizes from 12 nm to 20 nm and the molecular composition of the simulated systems is described in the supplemental information (tables 1 and 2). The simulation times were of the order of 500 ns.

Acknowledgements

This work utilized facilities at the National Institute for Standards and Technology, supported in part by the National Science Foundation under agreement No. DMR-0454672. U.P.-S and S.G

acknowledge support from U.S. Department of Energy, Office of Science, under contract No. DE-AC02-06CH11357. Certain commercial materials are identified in this paper to foster understanding. Such identification does not imply recommendation or endorsement by the National Institute of Standards and Technology, nor does it imply that the materials or equipment identified are necessarily the best available for the purpose. FCR acknowledges Centro Nacional de Supercomputo (CNS) del Instituto Potosino de Investigación Científica y Tecnológica (IPICYT) for its support with computing resources.

Notes and references

^a Materials Science Division, Argonne National Laboratory, Lemont, Illinois

^b Physics Department, University of Illinois at Chicago, Chicago, IL 60607, USA.

^c Centro de Investigación y de Estudios Avanzados del IPN, Mexico DF, Mexico

^d Large Scale Structure Group, Institut Laue-Langevin, Grenoble F-38042, France

^e Center for Neutron Research, National Institute of Standards and Technology, Gaithersburg, Maryland, MD 20899, USA

^f Department of Chemical Engineering, Colburn Laboratory, University of Delaware, Newark, Delaware

[‡] Present address: Berg LLC, Framingham, MA 01701, USA

E-mail: ursulaps@uic.edu

† Electronic Supplementary Information (ESI) available. See DOI: 10.1039/b000000x/

‡ http://avantlipids.com/index.php?option=com_content&view=article&id=1600&Itemid=381

‡‡ SANS measurements were performed on the NIST Center for Neutron Research NG3 30 m SANS instrument in Gaithersburg, Maryland and on D22 at the Institut Laue-Langevin (ILL) in Grenoble France. Data reduction and analysis using IGOR: S. R. Kline. 2006. Reduction and analysis of SANS and USANS data using IGOR Pro. *J Appl. Cryst.* 39(6):895; Data reduction using GRASP: <http://www.ill.eu/en/html/instruments-support/instruments-groups/groups/lss/grasp>; Data analysis using SANSVIEW: <http://danse.chem.utk.edu/sansview.html>

1. F. R. Maxfield and G. van Meer, *Current opinion in cell biology*, 2010, **22**, 422-429.
2. I. Tabas, *The Journal of clinical investigation*, 2002, **110**, 905-911.
3. F. R. Maxfield and I. Tabas, *Nature*, 2005, **438**, 612-621.
4. P. Duewell, H. Kono, K. J. Rayner, C. M. Sirois, G. Vladimer, F. G. Bauernfeind, G. S. Abela, L. Franchi, G. Nunez, M. Schnurr, T. Espevik, E. Lien, K. A. Fitzgerald, K. L. Rock, K. J. Moore, S. D. Wright, V. Hornung and E. Latz, *Nature*, 2010, **464**, 1357-1361.
5. J. Huang, J. T. Buboltz and G. W. Feigenson, *Biochimica et biophysica acta*, 1999, **1417**, 89-100.
6. M. M. Stevens, A. R. Honerkamp-Smith and S. L. Keller, *Soft matter*, 2010, **6**, 5882-5890.
7. S. R. Shaikh, V. Cherezov, M. Caffrey, S. P. Soni, D. LoCascio, W. Stillwell and S. R. Wassall, *Journal of the American Chemical Society*, 2006, **128**, 5375-5383.
8. M. R. Brzustowicz, V. Cherezov, M. Caffrey, W. Stillwell and S. R. Wassall, *Biophysical journal*, 2002, **82**, 285-298.
9. T. P. McMullen, R. N. Lewis and R. N. McElhaney, *Biophysical journal*, 2000, **79**, 2056-2065.

10. T. P. McMullen, R. N. Lewis and R. N. McElhaney, *Biochimica et biophysica acta*, 2009, **1788**, 345-357.
11. D. Bach and E. Wachtel, *Biochimica et biophysica acta*, 2003, **1610**, 187-197.
12. D. Bach, E. Wachtel, N. Borochoy, G. Senisterra, and R. M. Epand, *Chemistry and Physics of Lipids*, 1992, **63**, 105-113.
13. G. van Meer, D. R. Voelker and G. W. Feigenson, *Nature reviews. Molecular cell biology*, 2008, **9**, 112-124.
14. R. M. Epand, D. Bach, N. Borochoy and E. Wachtel, *Biophysical journal*, 2000, **78**, 866-873.
15. M. Raguz, L. Mainali, J. Widomska and W. K. Subczynski, *Biochimica et biophysica acta*, 2011, **1808**, 1072-1080.
16. J. Pan, F. A. Heberle, R. S. Petruzielo and J. Katsaras, *Chem Phys Lipids*, 2013, **170-171**, 19-32.
17. J. W. O'Connor and J. B. Klauda, *The journal of physical chemistry. B*, 2011, **115**, 6455-6464.
18. L. Miao, M. Nielsen, J. Thewalt, J. H. Ipsen, M. Bloom, M. J. Zuckermann and O. G. Mouritsen, *Biophysical journal*, 2002, **82**, 1429-1444.
19. M. Raguz, L. Mainali, J. Widomska and W. K. Subczynski, *Chem Phys Lipids*, 2011, **164**, 819-829.
20. N. Kucerka, J. Pencer, M. P. Nieh and J. Katsaras, *The European physical journal. E, Soft matter*, 2007, **23**, 247-254.
21. A. Hodzic, P. Zoumpoulakis, G. Pabst, T. Mavromoustakos and M. Rappolt, *Physical chemistry chemical physics : PCCP*, 2012, **14**, 4780-4788.
22. E. Plesnar, W. K. Subczynski and M. Pasenkiewicz-Gierula, *The journal of physical chemistry. B*, 2013, **117**, 8758-8769.
23. R. Ziblat, I. Fargion, L. Leiserowitz and L. Addadi, *Biophysical journal*, 2012, **103**, 255-264.
24. J. B. Lim, B. Rogaski and J. B. Klauda, *The journal of physical chemistry. B*, 2012, **116**, 203-210.
25. M. D. Daily, B. N. Olsen, P. H. Schlesinger, D. S. Ory and N. A. Baker, *Journal of chemical theory and computation*, 2014, **10**, 2137-2150.